Cell migration without a lamellipodium: translation of actin dynamics into cell movement mediated by tropomyosin

Stephanie L. Gupton,[1] Karen L. Anderson,[2] Thomas P. Kole,[3] Robert S. Fischer,[1] Aaron Ponti,[1] Sarah E. Hitchcock-DeGregori,[4] Gaudenz Danuser,[1] Velia M. Fowler,[1] Denis Wirtz,[3] Dorit Hanein,[2] and Clare M. Waterman-Storer[1]

[1]Department of Cell Biology, The Scripps Research Institute, La Jolla, CA 92037
[2]Program on Cell Adhesion, The Burnham Institute, La Jolla, CA 92037
[3]Department of Chemical and Biomolecular Engineering, Johns Hopkins University, Baltimore, MD 21218
[4]Department of Neuroscience and Cell Biology, Robert Wood Johnson Medical School, University of Medicine and Dentistry of New Jersey, Piscataway, NJ 08854

The actin cytoskeleton is locally regulated for functional specializations for cell motility. Using quantitative fluorescent speckle microscopy (qFSM) of migrating epithelial cells, we previously defined two distinct F-actin networks based on their F-actin–binding proteins and distinct patterns of F-actin turnover and movement. The lamellipodium consists of a treadmilling F-actin array with rapid polymerization-dependent retrograde flow and contains high concentrations of Arp2/3 and ADF/cofilin, whereas the lamella exhibits spatially random punctae of F-actin assembly and disassembly with slow myosin-mediated retrograde flow and contains myosin II and tropomyosin (TM). In this paper, we microinjected skeletal muscle αTM into epithelial cells, and using qFSM, electron microscopy, and immunolocalization show that this inhibits functional lamellipodium formation. Cells with inhibited lamellipodia exhibit persistent leading edge protrusion and rapid cell migration. Inhibition of endogenous long TM isoforms alters protrusion persistence. Thus, cells can migrate with inhibited lamellipodia, and we suggest that TM is a major regulator of F-actin functional specialization in migrating cells.

Introduction

Cell migration is thought to occur by a coordinated cycle of leading edge protrusion in the direction of migration, substrate adhesion of the protrusion, generation of tension on new adhesions to advance the cell body, and de-adhesion of the trailing cell rear. F-actin is required for each step of the cycle. Spatio-temporally coordinated regulation of the interaction of F-actin with specific binding proteins and myosin motors is required for the actin cytoskeleton to perform such diverse mechanical functions.

Using computational quantitative analysis of fluorescent speckle microscopy (FSM) movies of F-actin in migrating epithelial cells, we showed two distinct arrays of F-actin exist at the leading edge, the lamellipodium, and the lamella (Ponti et al., 2004). Quantitative FSM (qFSM) analysis produces spatio-temporal maps of F-actin assembly/disassembly (kinetics) and motion (kinematics) by tracking the position and intensity

fluctuations of fluorescent actin speckles in FSM movies (Waterman-Storer et al., 1998, Danuser and Waterman-Storer, 2003, Vallotton et al., 2003, Ponti et al., 2003, 2004). The two distinct F-actin arrays are operationally defined by four criteria: (1) the molecules that differentially localize to them (their molecular signatures), (2) the spatial organization of the rates of F-actin assembly/disassembly (their kinetic signatures), and (3) the rate and (4) mechanism of F-actin meshwork translocation (their kinematic signatures; Ponti et al., 2004).

The lamellipodium kinetic signature is characterized by fast F-actin polymerization subjacent to the leading edge, followed by near complete filament depolymerization a few micrometers back, creating a 2–4-μm-wide treadmilling actin array abutting the cell edge (Watanabe and Mitchison, 2002; Ponti et al., 2004). This kinetic behavior may be mediated by the signature molecules concentrated in this region, Arp2/3 and ADF/cofilin, with F-actin nucleated from existing filaments by the Arp2/3 complex and ADF/cofilin mediating filament severing (Bailly et al., 1999; Svitkina and Borisy, 1999; Pollard et al., 2000). Severed filaments contribute to depolymerization from

Correspondence to Clare Waterman-Storer: waterman@scripps.edu
Abbreviations used in this paper: FSM, fluorescent speckle microscopy; qFSM, quantitative FSM; skTM; skeletal muscle αTM; TM, tropomyosin.
The online version of this article includes supplemental material.

Supplemental Material can be found at:
http://www.jcb.org/cgi/content/full/jcb.200406063/DC1

"pointed" ends (Carlier et al., 1997; Svitkina and Borisy, 1999) and creation of new fast growing "barbed" ends (Ichetovkin et al., 2002). Monomer addition at F-actin barbed ends is thought to provide the force for leading edge protrusion (Tilney et al., 1981; Mogilner and Oster, 2003) and also drives the rapid retrograde flow ($\sim$1 μm/min) of the F-actin meshwork that marks the kinematic signature of the lamellipodium (Waterman-Storer et al., 1998; Salmon et al., 2002; Vallotton et al., 2003; Ponti et al., 2004).

The lamella of migrating epithelial cells comprises an area within 3–15 μm from the cell edge. Lamella actin kinetics are marked by spatially discrete foci of polymerization and depolymerization, which aphasically cycle between these states (Ponti et al., 2004). Myosin II–dependent (Lin et al., 1996; Ponti et al., 2004) slow retrograde flow ($\sim$0.3 μm/min; Waterman-Storer et al., 1998; Salmon et al., 2002) defines the kinematic signature of the lamella F-actin, which may be mediated by the other signature molecule in this region, tropomyosin (TM; Ponti et al., 2004). Both myosin II and TM are absent from the lamellipodium (Lazarides, 1976; DesMarais et al., 2002; Ponti et al., 2004). In the cell body, F-actin undergoes myosin-dependent anterograde flow, which meets F-actin retrograde flow from the lamella in a region of filament depolymerization but little actin motion termed the "convergence zone" (Gupton et al., 2002; Salmon et al., 2002). The junction between the lamellipodium and lamella is marked by substrate adhesions (Izzard and Lochner, 1980; Ponti et al., 2004), which are transmembrane complexes of integrins, signaling proteins, and actin binding proteins that translate actomyosin contraction in the lamella into cell pulling forces on the ECM.

We showed that persistent leading edge advance was associated with forward expansion of the lamella F-actin network, whereas kinetic and kinematic changes in the lamellipodium correlated only with cyclic, short-lived leading edge protrusion and retraction (Ponti et al., 2004). This finding suggested the lamella actin array is critical to productive cell advance, questioning the importance of the lamellipodium for cell migration. In the present work, we sought to alter the identity of F-actin arrays near the leading edge of migrating cells to determine their functional contribution to cell motility.

TM is a good candidate protein whose mislocalization could change the identity of F-actin arrays in migrating cells. In vitro studies have shown nonmuscle and skeletal TMs block Arp2/3 nucleating (Blanchoin et al., 2001) or ADF/cofilin severing of F-actin (Bernstein and Bamburg, 1982) and inhibit pointed-end depolymerization (Broschat, 1990). TMs regulate myosin II interactions with F-actin as characterized in skeletal muscle. Thus, TMs could be central to distinguishing lamella and lamellipodium F-actin arrays by inhibiting F-actin binding by lamellipodium signature proteins (DesMarais et al., 2002) and promoting association of lamella proteins like myosin II. Here, we microinjected purified skeletal muscle αTM (skTM) as a specific tool to alter distinct F-actin arrays near the leading edge of migrating cells to determine their contribution to cell migration.

Results

High levels of skTM localize to the leading edge of PtK₁ cells

We used PtK₁ epithelial cells, whose F-actin organization, kinetics, and kinematics we have extensively characterized (Wittmann et al., 2003; Ponti et al., 2004). In small islands (Fig. 1 A), the noncontacted edges of these cells exhibit protrusive and retractive activity and as a group undergo random motility at 0.55 ± 0.03 μm/min. The F-actin cytoskeleton consists of a dense F-actin meshwork at the cell edge that thins at 2–4 μm from the edge, followed by transverse bundles (Fig. 1 D; Wittmann et al., 2003; Ponti et al., 2004). Whole-mount EM reveals two morphologically distinct networks near the cell edge (Fig. 1 F). In the region 2–4 μm from the cell edge is a homogenous isotropic filament network (Fig. 1 G), whereas more proximal regions contain denser filament bundles that extend toward the leading edge and are interspersed by isotropic network. These structurally distinct networks likely correspond to the lamellipodium and lamella, respectively, as defined previously by their molecular, kinetic, and kinematic signatures (Ponti et al., 2004).

Nonmuscle cells generally express multiple TM isoforms differentially spliced from four genes (Lin et al., 1997). Exon-specific antibodies revealed that PtK₁ cells expressed at least one long ($\sim$39 kD) and one short ($\sim$36 kD) isoform of TM, one of which was recognized by the CG3 monoclonal antibody specific for TM5 or TM5NM (Fig. 1 B). Immunofluorescence using a long TM-specific monoclonal antibody (TM311; Fig. 1 D) or a TM polyclonal antibody to long and short isoforms (RB14; not depicted) showed TM localization to F-actin bundles in the cell body and lamella, but exclusion 2–4 μm from the leading edge (Fig. 1 D) as reported for other cell types (DesMarais et al., 2002).

To increase TM levels in PtK₁ cells, we microinjected rabbit psoas αTM (skTM; Fig. 1 C) at a needle concentration of $\sim$140 μM resulting in an intracellular concentration well above the F-actin Kd. Using a striated muscle TM-specific antibody, we found that skTM localized to F-actin in the lamella and bundles in the cell center, but in contrast to endogenous TMs, skTM extended to the leading edge (Fig. 1 E). This antibody did not recognize endogenous TMs in PtK₁ cells (Fig. 1 B). Cells containing skTM showed increased F-actin bundles extending from the cell body to the leading edge or beyond, creating filopodial-like protrusions that were not present in control cells (Fig. 1 E, arrowhead). EM of skTM-injected cells revealed loss of the homogenous, isotropic filament array typical of the lamellipodium, and filaments in an ordered array of bundles (Fig. 1, H and I, yellow) oriented toward the leading edge similar to the lamella of control cells, often with more filopodia-like protrusions (Fig. 1 G, arrows). Stereo-imaging indicated that cells injected with skTM have a much thinner lamella than control cells (Fig. S1, available at http://www.jcb.org/cgi/content/full/jcb.200406063/DC1).

To determine how mislocalization of TM to the leading edge affected the organization of F-actin into lamellipodium and lamella, we further characterized the leading edges of
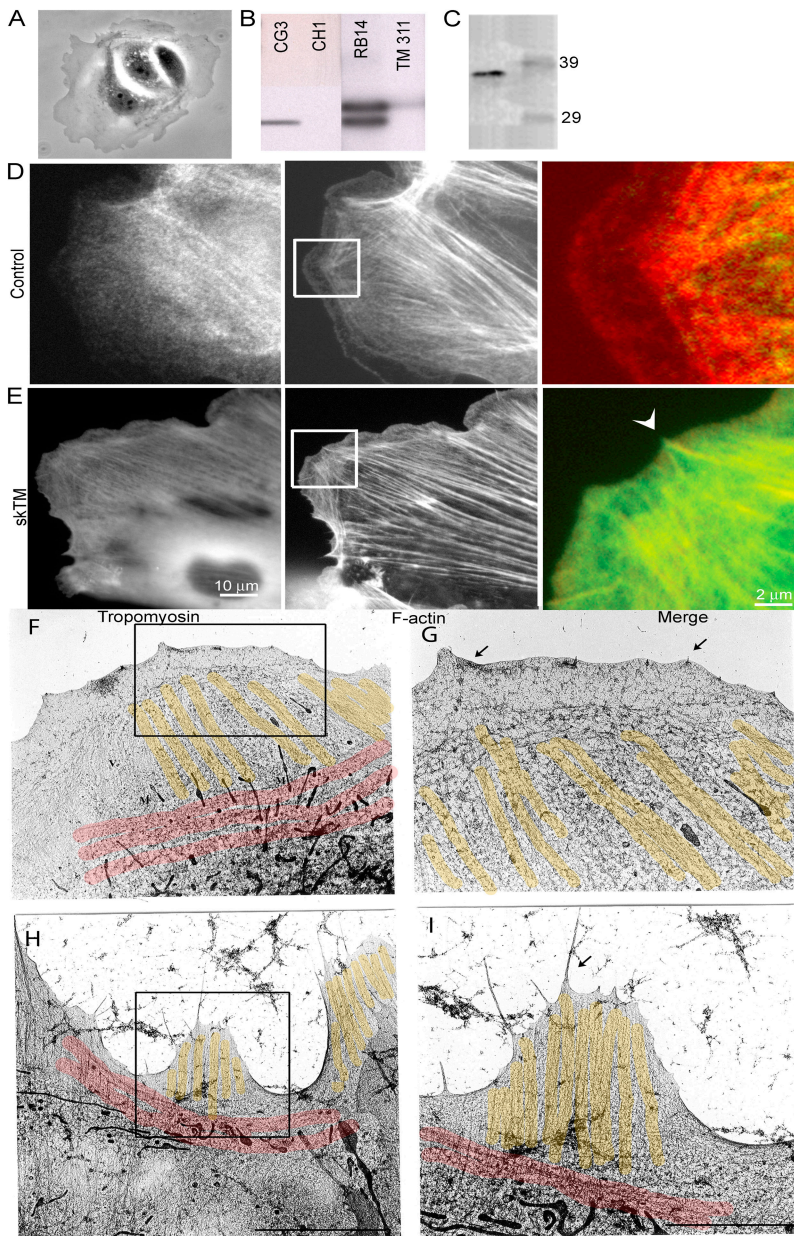
Figure 1. **skTM localizes to F-actin throughout the cell.**
(A) Island of PtK$_1$ epithelial cells. (B) Western blot analysis of PtK$_1$ lysate for TM isoforms. (C) Purified skTM seen by Coomassie blue. Numbers refer to mass markers. (D) Immunolocalization of long TMs (TM311 monoclonal) and F-actin (fluorescent phalloidin) in a PtK$_1$ cell. TM is excluded from the cell edge. (E) PtK$_1$ cell injected with skTM and immunolabeled with muscle-specific CH1 antibody and costained for F-actin. Filopodial-like protrusions occur in cells injected with skTM (arrowhead). Merged images in D and E are from boxed regions, with F-actin and TM in red and green, respectively. Whole mount EM of control (F and G) and skTM-injected (H and I) cells. G and I show enlargements of F and H, respectively. Near the cell edge, an isotropic network and small vertical ruffles (arrows) are present, followed by the lamella with dense population of bundles (yellow) oriented toward the cell margin. A horizontal dense belt of filaments (red) delineate the cell body from the lamella (red). In the injected cell (H), the only visible network is comprised of oriented bundles (yellow) and filopodia-type protrusions (arrow in I). Bars: (F and H) 2.4 μm; (G and I) 5.0 μm.

skTM-injected cells according to their: (a) molecular signatures, (b) spatial organization of the rates of F-actin assembly/disassembly (kinetic signatures), and (c) rate and (d) mechanism of F-actin meshwork translocation (kinematic signatures).

skTM depletes Arp2/3 and ADF/cofilin from the leading edge and decreases local free barbed filament ends

To determine if skTM affected Arp2/3 and ADF/cofilin targeting to the cell edge, their localizations were examined by immunofluorescence. Control cells had Arp2/3 and ADF/cofilin throughout the cell, with the highest concentration within 2–4 μm from the leading cell edge (Fig. 2, A and C), as previously reported (Welch et al., 1997; Svitkina and Borisy, 1999; Ponti et al., 2004). In contrast, cells containing skTM had less Arp2/3 and ADF/cofilin at the leading edge (Fig. 2, B and D). To quan-

tify this, fluorescence intensity along line scans from the cell edge into the cell center were measured (13 cells per treatment, three measurements per cell). This conclusively showed cells containing skTM had a twofold decrease in Arp3 and ADF/cofilin relative to F-actin along these profiles (Fig. 2 E) due to major decreases in Arp3 and ADF/cofilin near the cell edge and increases in F-actin toward the cell center (Fig. 2, F and G).

Because Arp2/3 and ADF/cofilin are thought to supply polymerization-competent free barbed filament ends to the lamellipodium (for review see Pollard et al., 2000), we analyzed the localization and amount of free barbed ends (see Materials and methods). In control cells, free barbed ends were in a narrow rim along the leading edge (Symons and Mitchison, 1991), and at the end of F-actin bundles, likely at substrate adhesions (Fig. 3 A). In contrast, free barbed ends at the leading edge were dramatically reduced in cells containing skTM (Fig. 3 C),
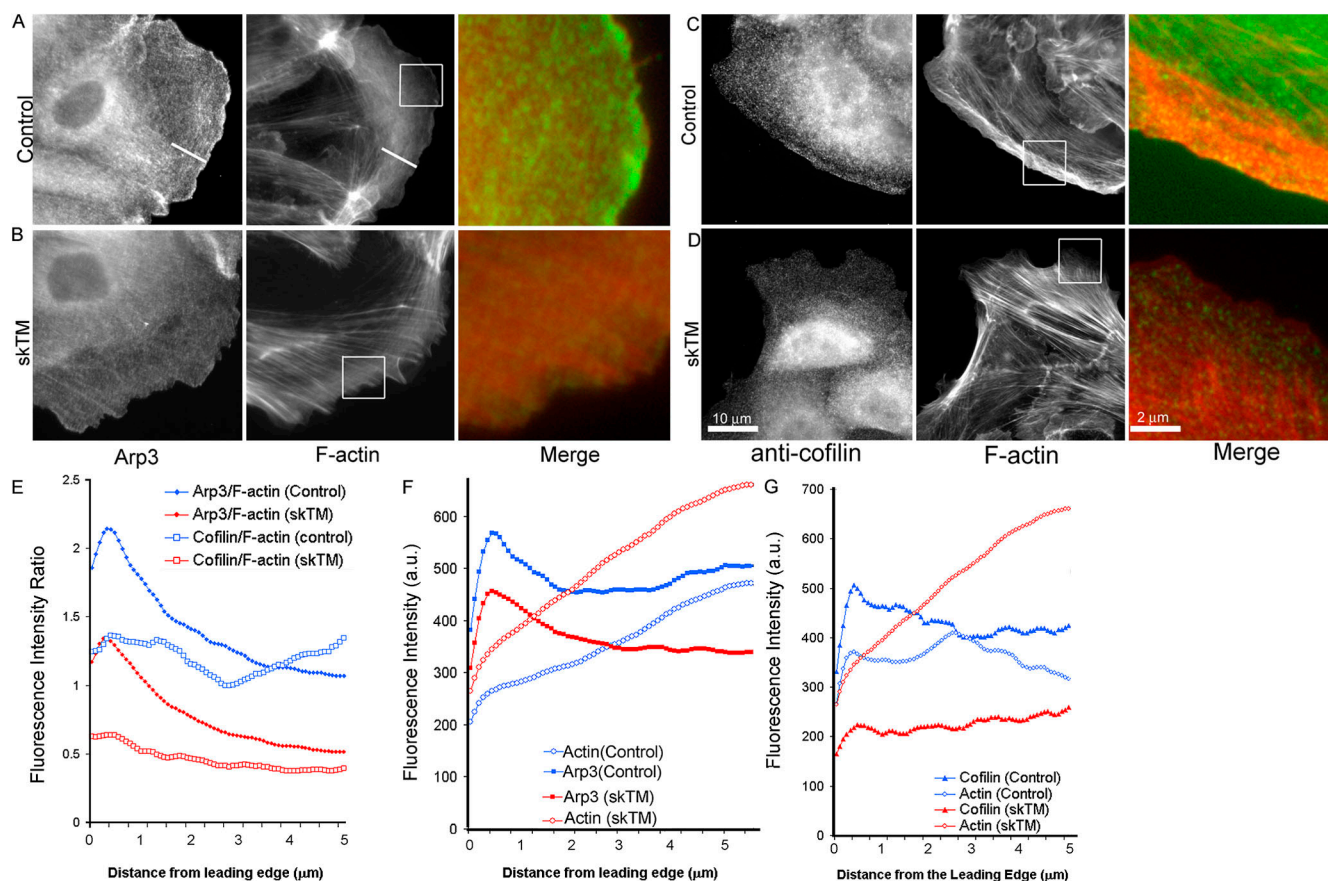
Figure 2. **skTM depletes Arp2/3 and ADF/cofilin from the leading edge of PtK₁ cells.** (A) Immunolocalization of Arp3 and F-actin (fluorescent phalloidin) in control cells (A) and cells injected with skTM (B). Lines in A are examples of one region where fluorescence intensity line scans were taken to produce the type of data seen in E and F. ADF/cofilin and F-actin localization in control cells (C) and cells injected with skTM (D). Boxed regions are magnified in the Merge column, with Arp3 (A and B) and ADF/cofilin (C and D) in green and F-actin in red. (E) Average fluorescence intensity ratio of Arp3/F-actin and cofilin/F-actin in control and skTM-injected cells measured from the cell edge (0 μm) into the cell center. Fluorescence intensity of Arp3 (F) or ADF/cofilin (G) and F-actin staining in control and skTM-injected cells measured from the cell edge (0 μm) into the cell center. In E–G, data are averaged from 13 cells per treatment, three measurements per cell.

although some persisted at filopodial tips and in adhesions (Fig. 3 B). Analysis of fluorescence along line scans from the leading edge into the cell center quantitatively confirmed this (Fig. 3, C and D, three measurements per cell, 13 cells per treatment).

Immunofluorescence localization of the barbed-end protecting proteins Mena or VASP or the "leaky cap" mDia2 showed no differences in cells containing skTM versus controls (Fig. S2, available at http://www.jcb.org/cgi/content/full/jcb.200406063/DC1), suggesting barbed ends remaining in skTM cells may be protected. The localization of filamin and cortactin was unaffected by skTM (Fig. 3), indicating a specific effect on Arp2/3 and cofilin localization.

Kinetic and kinematic analysis of F-actin dynamics reveals skTM inhibits lamellipodium formation

To determine the effects of skTM on the kinetics and kinematics of the actin cytoskeleton, we performed time-lapse spinning-disk confocal imaging of cells injected with low levels of X-rhodamine–labeled actin (Fig. 4 C and Video 1, available at http://www.jcb.org/cgi/content/full/jcb.200406063/DC1) and performed qFSM image analysis of protrusive cells (Waterman-Storer et al.,

1998; Danuser and Waterman-Storer, 2003; Vallotton et al., 2003; Ponti et al., 2003). Control cells displayed a treadmilling lamellipodial array seen as a discrete narrow band of rapid F-actin polymerization (Fig. 4 A, red arrow) along the leading edge juxtaposed against a narrow band of rapid F-actin depolymerization (Fig. 4 A, green, $n = 4$ cells; and Video 2, available at http://www.jcb.org/cgi/content/full/jcb.200406063/DC1). In the lamella, 1–3-μm-diam foci of polymerization and depolymerization were intermixed (Fig. 4 A and Video 2; Ponti et al., 2003, 2004). In contrast, qFSM analysis of F-actin kinetics in cells containing skTM revealed a single region of lamella-like kinetic behavior throughout the cell (Fig. 4 A, skTM; and Video 2, $n = 4$ cells). These cells completely lacked the bands of polymerization and depolymerization at the leading edge typical of the treadmilling actin array of the lamellipodium. Similarly, inhibition of Arp2/3 by the CA domain of the Arp2/3 activator N-Wasp (Strasser et al., 2004) caused the disappearance of the juxtaposed bands of polymerization and depolymerization at the cell edge (Fig. 4 A, GFP-CA). It should be noted that the dramatic difference in F-actin kinetics produced by these different perturbations are not at all apparent from the morphology of the cell edge as seen by phase contrast, but are only revealed by qFSM analysis.
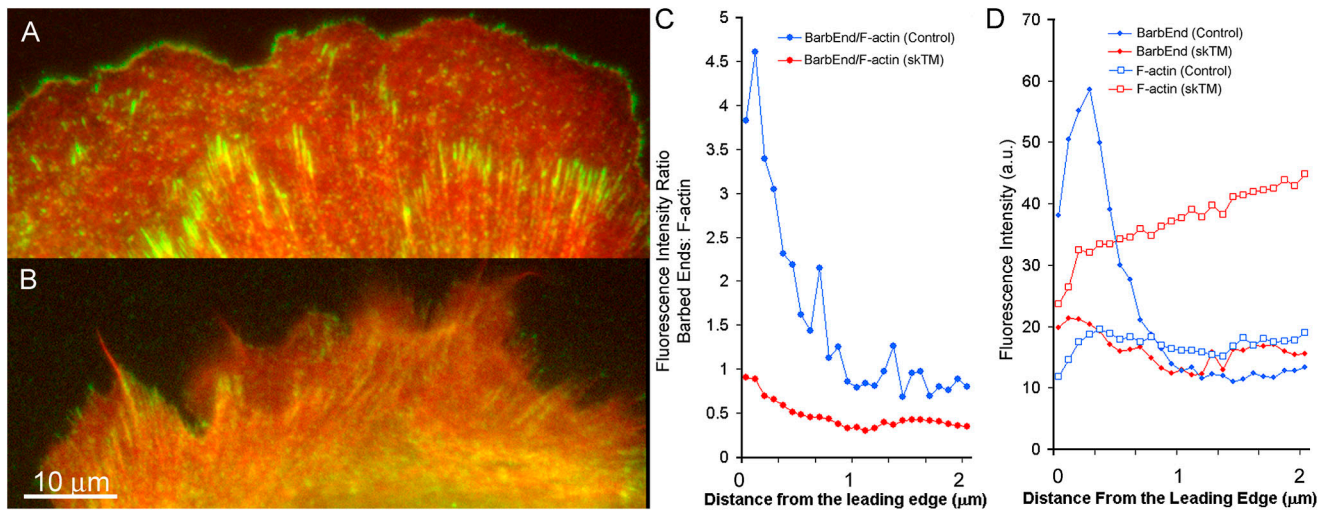
Figure 3. **skTM decreases the concentration of polymerization-competent free barbed filament ends at the cell edge.** Barbed-end actin incorporation (green) and fluorescent phalloidin (red) in a control cell (A) and an skTM-injected cell (B). (C) Intensity ratio of fluorescent actin incorporation marking free barbed filament ends relative to F-actin. (D) Intensity of fluorescent actin incorporation marking free barbed ends and F-actin staining. Profiles in C and D were measured from line scans taken from the cell edge (0 μm) into the cell center and data are averaged from 14 cells per treatment, three measurements per cell.

We used kymograph analysis of F-actin FSM movies (Video 1) to characterize F-actin kinematics (Fig. 4, C and D) and their segregation into spatially distinct regions (Fig. 4 G and Table I). In control cells, F-actin underwent fast retrograde flow (0.688 ± 0.334 μm/min, $n = 5$ cells, 137 measurements) in a band 1.57 ± 0.09-μm-wide at the leading edge, typical of a lamellipodium. In a 11.7 ± 0.8-μm-wide region behind the lamellipodium, F-actin exhibited lamella signature kinematics characterized by slow retrograde flow (0.253 ± 0.138 μm/min; Fig. 4 G, $n = 5$ cells, 163 measurements). An F-actin convergence rate of 0.44 μm/min was calculated by summing the average rate of lamella retrograde and cell body anterograde flow (0.19 ± 0.26 μm/min; Fig. 4 G, $n = 5$ cells, 158 measurements).

In contrast to control cells, cells with skTM had only one distinct region of F-actin kinematics at the cell edge. This 12.8 ± 0.9-μm-wide region exhibited retrograde flow at 0.885 ± 0.264 μm/min ($n = 4$ cells, 138 measurements; Fig. 4, D and G; and Video 1), which is not significantly different from the lamellipodium rate of control cells. The rapid F-actin retrograde flow met increased anterograde flow (0.25 ± 0.17 μm/min, $n = 4$ cells, 42 measurements), resulting in an F-actin convergence rate three times faster than control cells (1.14 μm/min). The convergence zone, defined by the lack of directed F-actin movement, was three times wider in skTM-containing cells than in controls (Table I).

Because molecular localization and qFSM kinetic analyses suggested skTM inhibited lamellipodium formation, whereas kinematic kymograph analysis suggested lamella inhibition, we used drug sensitivity to identify the mechanism driving retrograde flow to clarify this controversy. Retrograde flow in the lamellipodium is dependent on F-actin treadmilling as it is inhibited by cytochalasin D and jasplakinolide, which are drugs that modulate F-actin assembly/disassembly, and is unaffected by drugs that inhibit myosin II activity, whereas lamella retrograde flow is sensitive to myosin II inhibitors (Gupton et al., 2002; Ponti et al., 2004). Retrograde flow in cells containing skTM was

unaffected by cytochalasin D (Fig. 4 E) but was immediately arrested by blebbistatin (Fig. 4 F), indicating the single region of F-actin kinematics was myosin II dependent and therefore operationally defined as a lamella. However, the rate of lamella retrograde flow in cells containing skTM was ~3.5 times faster than lamella flow in control cells (Fig. 4 G, P < 0.0001).

skTM-induced changes in F-actin kinematics are due to increased myosin II decoration of F-actin

To determine if the increased rate of F-actin retrograde flow and convergence in cells containing skTM was due to altered myosin II recruitment, myosin IIA heavy chain and F-actin were localized in control and skTM-injected cells. In control cells, myosin IIA was excluded from the lamellipodium (Ponti et al., 2004), and appeared in a gradient of punctae within the lamella (Fig. 5 A; Verkhovsky et al., 1995). In cells containing skTM, myosin IIA punctae often extended all the way to the leading edge of the cell (Fig. 5 B), mirroring skTM distribution (Fig. 1 E). The ratio of myosin IIA/F-actin from the leading edge toward the cell center was quantified by line scan analysis, indicating cells with skTM have increased myosin II levels at their cell edges (Fig. 5, C and D, three measurements per cell, 14 cells per treatment).

A lamellipodium is dispensable for persistent protrusion and cell migration in the presence of high levels of skTM

Changes in localization of signature molecules, F-actin kinetic analysis, and drug sensitivity of F-actin kinematics suggests that skTM inhibits lamellipodium formation, leaving behind a leading edge lamella with increased myosin II–dependent F-actin flow. We cannot rule out that lamellipodia, which are very transient or not resolvable by our criteria, still exist, but we suggest that such possible residual lamellipodia would make minimal contribution to cell behavior. To test whether or not the lamelli-

Figure 4. skTM inhibits the formation of the lamellipodium. (A) F-actin turnover maps computed from qFSM time-lapse movies and corresponding phase-contrast images in a control, an skTM-injected (skTM), and a GFP-CA-expressing (GFP-CA) cell. Turnover maps depict polymerization (red) and depolymerization (green) rates. Control cells exhibit narrow bands of fast polymerization and depolymerization in the lamellipodium adjacent to the leading edge (arrow) and spatially random punctae of polymerization and depolymerization in the lamella. Cells containing skTM or GFP-CA exhibit lamella F-actin kinetics at their edges (arrows). (B) FSM image of F-actin in a control PtK$_1$. White line shows location used to generate kymograph in C. (C and D) Kymographs of a control (C) and an skTM-injected (D) cell; white lines highlight speckle translocation used to calculate flow velocities. There are two regions of distinct retrograde flow rates in controls and only one region of retrograde flow in cells containing skTM. (E and F) Kymographs taken from F-actin FSM time series of skTM-containing cells. In E, at the first arrowhead, 200 nM cytochalasin D was perfused and washed out at the second arrowhead. Arrows illustrate leading edge protrusive behavior; lines emphasize retrograde flow rates. In cytochalasin D, leading edge protrusion stops, but retrograde F-actin flow continues. In F, 100 μM blebbistatin was perfused at the arrowhead; lines emphasize actin flow rates. After treatment, retrograde and anterograde F-actin flow immediately arrested. (G) Average F-actin flow rates in different cellular regions taken from kymographs of control (blue) and skTM-injected cells (red) (bars equal SEM). Negative and positive flow rates imply retrograde and anterograde flow, respectively. Convergence rate is the sum of the absolute value of average lamella retrograde flow and cell body anterograde flow.
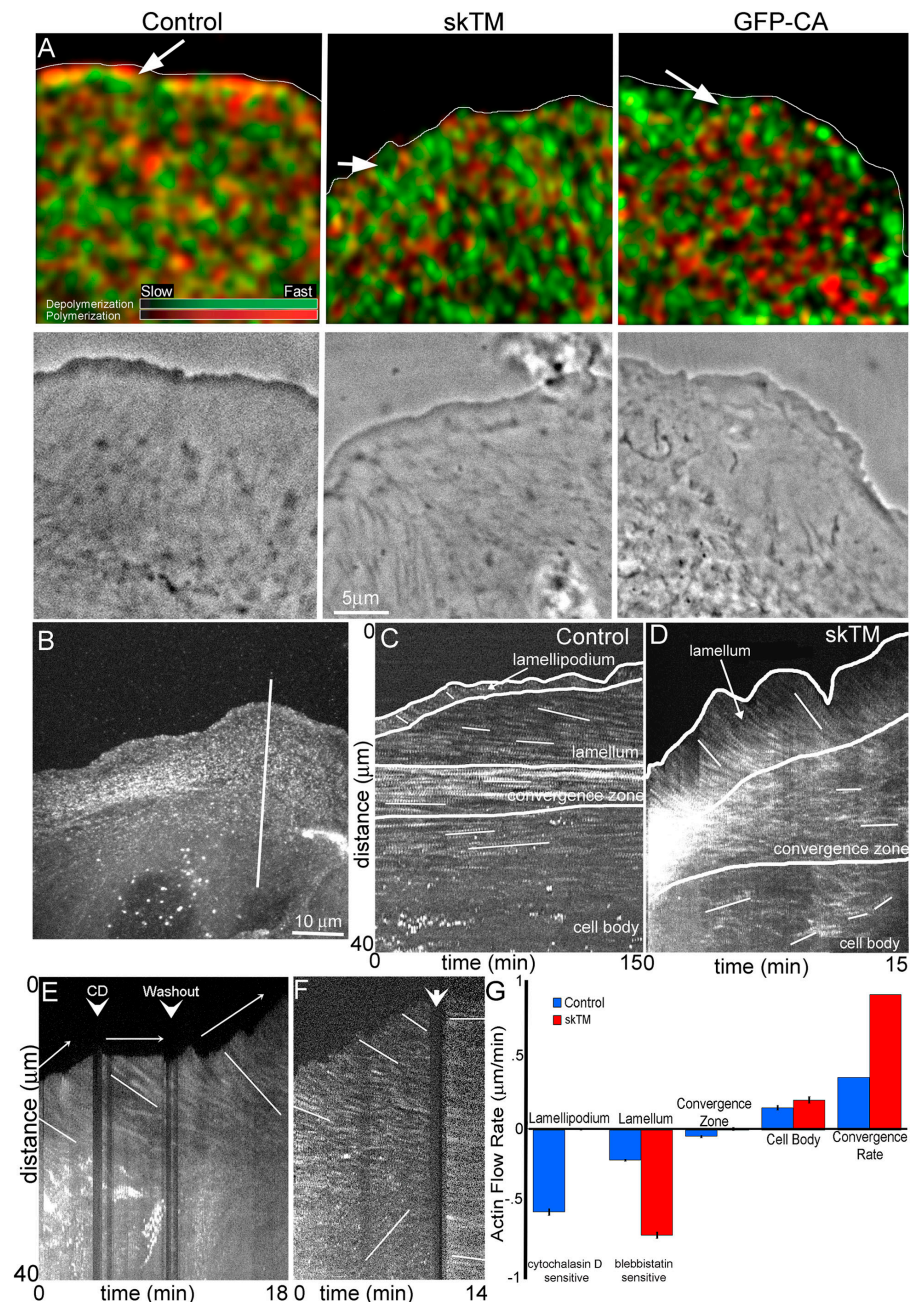
podium is required for cell motile function, we used phase-contrast microscopy to analyze leading edge behavior and migration velocity of cells containing skTM (Video 3, available at http://www.jcb.org/cgi/content/full/jcb.200406063/DC1). Leading edge protrusion and retraction were analyzed by kymograph (Table II and Fig. 6) and showed that rates in control and skTM-injected cells were not significantly different (Table II). However, cells injected with skTM exhibited a twofold increase in protrusion persistence time and a decreased retraction persistence compared with controls (Table II). In contrast, cells expressing the CA domain of N-Wasp, which inhibits Arp2/3 (Brieher et al., 2004; Strasser et al., 2004), have similar protrusion persistence as controls, although the rate of protrusion is significantly slower. Analysis of cell velocity demonstrated that islands in which all cells were injected with skTM migrated twice as fast ($n = 113$

cells) as islands of controls ($n = 73$ cells, P < 0.0001; Table II and Fig. 6). In contrast, inhibition of lamellipodium formation with CA resulted in cell motility indistinguishable from controls.

Changes in cell migration correlate with changes in substrate adhesion distribution and dynamics and cytoplasm viscoelasticity

One hypothesis to explain enhanced migration of cells containing skTM is by contraction-mediated promotion of adhesion distribution and/or turnover (Chrzanowska-Wodnicka and Burridge, 1996; Webb et al., 2004). In controls, the adhesion marker paxillin was in plaques at the ends of F-actin bundles likely at the lamellipodium–lamella junction (Ponti et al., 2004; Fig. 7 A). In cells containing skTM, paxillin also localized to punctae along bundles in the cell body (Fig. 7 B, arrowhead;

Table I. skTM changes the organization of kinematically distinct regions of the actin cytoskeleton

	Lamellipodium width	Lamella width	Convergence zone width
	μm	μm	μm
Control cells	1.57 ± 0.09	11.7 ± 0.8	5.3 ± 0.16
n = 5 cells	n = 132 measurements	n = 66 measurements	n = 134 measurements
skTM cells	0	12.8 ± 0.9	15.4 ± 0.86
n = 5 cells	n = 106 measurements	n = 54 measurements	n = 80 measurements
P-value	<.0001	0.66	<.0001

Width measurements of each region were made from kymographs of F-actin FSM movies and averaged for multiple measurements (five cells per treatment, approximately three kymographs per cell). Regions were defined by the rate and drug sensitivity of their retrograde flow (see text). Numbers are averages ± SEM.

and Video 4, available at http://www.jcb.org/cgi/content/full/jcb.200406063/DC1), suggesting their engagement to the substrate at sites along their lengths. In addition, adhesions were located 36% closer to the leading edge (1.9 ± 0.16 μm) compared with control cells (2.6 ± 0.16 μm, P = 0.003; Fig. 7 C) and were more dynamic than in control cells (Video 4, arrows).

One possible explanation for enhanced protrusive persistence of cells containing skTM is changes in the stiffness of the lamella actin network. To investigate the mechanical properties of the cytoplasm we used intracellular microrheology to probe in situ local intracellular viscoelasticity. This force-free method transforms measured Brownian displacements of injected microspheres in the cytoplasm (Fig. 8, A and B) into local viscous and elastic moduli (Mason et al., 1997; Apgar et al., 2000; Dasgupta et al., 2002). This revealed a greater than fivefold (P < 0.05) increase in the stiffness of the lamella of skTM-injected cells compared with controls (Fig. 8 C).

Endogenous long TMs organize actomyosin contractility

To investigate the role of endogenous TM, we inhibited long TMs by microinjecting a long TM-specific monoclonal antibody (TM311; Nicholson-Flynn et al., 1996) that recognized a single band of ~39 kD (Fig. 1 B) and immunolocalized along F-actin bundles and in punctae in the lamella of controls (Fig. 1 D

and Fig. 9 A). In contrast, injected TM311 antibody did not localize to F-actin structures but was diffuse in the cytoplasm (Fig. 9 B), suggesting the antibody inhibited TM–F-actin interactions. In addition, injected cells had decreased density and straightness of F-actin bundles in the cell center (Fig. 9, A and B).

Kymograph analysis of F-actin FSM movies showed antibody inhibition of long TMs decreased lamella retrograde flow rate 35% compared with control (0.17 ± 0.072 vs. 0.26 ± 0.127 μm/min, P < 0.0001), decreasing the F-actin convergence rate (Fig. 9 C). In addition, TM inhibition altered protrusion directional persistence, which was normally confined to one leading edge over many hours. Cells with inhibited long TMs sent out multiple protrusions that switched from site to site over the course of minutes (Video 5, available at http://www.jcb.org/cgi/content/full/jcb.200406063/DC1). Immunostaining of antibody-injected cells showed no obvious changes in the localization and distribution of Arp2/3, ADF/cofilin, or myosin II (unpublished data).

Discussion

Cell migration without a lamellipodium

In this paper, we showed that introducing high levels of skTM into migrating epithelial cells caused major alterations in the organization and dynamics of the actin cytoskeleton, which
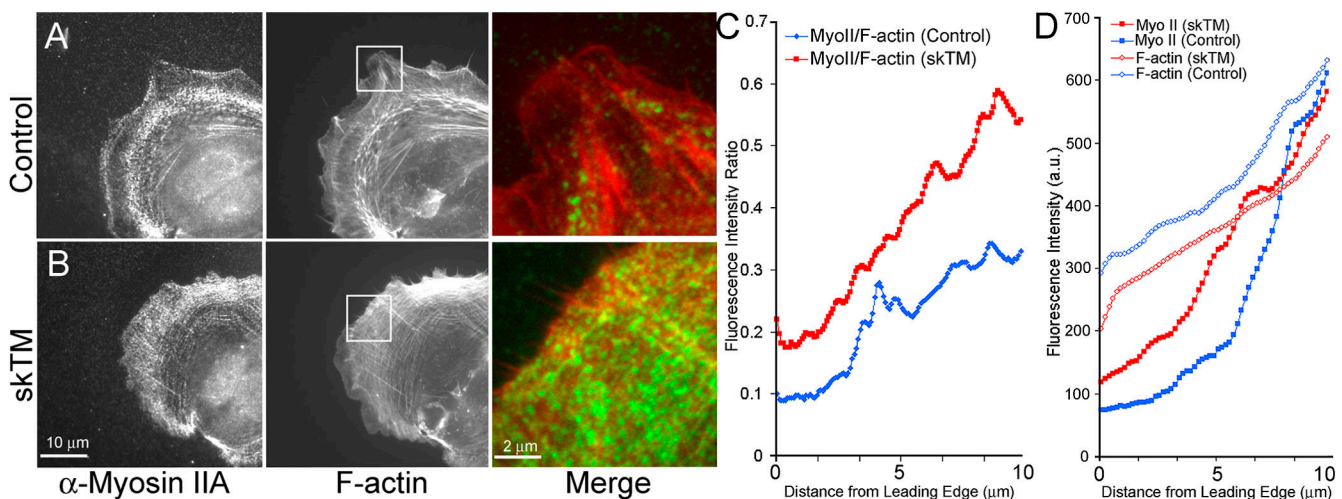
Figure 5. **skTM recruits myosin IIA to the leading edge.** Immunolocalization of myosin IIA heavy chain and fluorescent phalloidin staining of F-actin in a control (A) and an skTM-injected (B) PtK₁ cell. The insets are magnified in the right column, with F-actin red and myosin IIA green. (C) Intensity ratio of myosin IIA/F-actin in control and skTM-injected cells measured from the cell edge (0 μm) into the cell center. (D) Fluorescence intensity of myosin IIA and F-actin staining in control and skTM-injected cells measured from the cell edge (0 μm) into the cell center. In C and D, data are averaged from 14 cells, three measurements per cell.

Figure 6. **skTM increases leading edge protrusion persistence and cell migration velocity.** Phase-contrast images (left column) and kymographs (right two columns) taken from movies of leading edges of control cells (top row) and skTM-injected cells (bottom row). White lines depict locations used to generate kymographs. Arrowheads delineate the beginning of each retraction phase. Graph displays average instantaneous cell migration velocity in control, skTM-injected (skTM), and GFP-CA (CA)–expressing PtK$_1$ cell islands. *, $P < 0.01$.
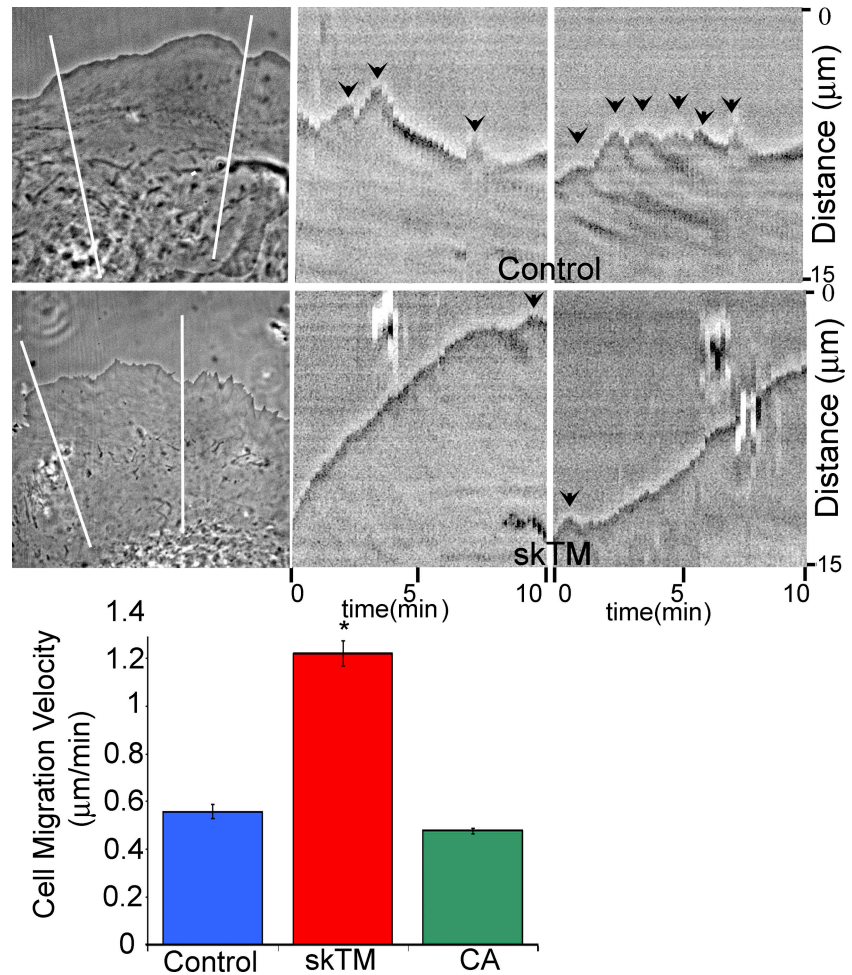
translated into changes in cell morphology and migratory behavior. Specifically, skTM inhibited the formation of the leading edge lamellipodium as determined by several criteria: displacing its signature molecules Arp2/3 and ADF/cofilin; inhibiting the signature F-actin kinetics of juxtaposed bands of polymerization/depolymerization at the cell edge; and inhibiting the cytochalasin-sensitive region of F-actin retrograde flow kinematics. Loss of the lamellipodium allowed the lamella F-actin array to extend to the cell edge. Although we cannot rule out that a lamellipodium that is transient or not resolvable by our criteria still exists, cells containing skTM with inhibited lamellipodia exhibited persistent leading edge protrusion and rapid cell migration, indicating a lamellipodium and rapid actin treadmilling at the leading edge are unnecessary for these cell motile functions. This finding was corroborated by inhibition of lamellipodium formation by disruption of Arp2/3 complex function with the CA domain of WASP. Because our results indicate that a lamellipodium is dispensable for leading edge protrusion and migration, we suggest that the lamellipodium may be required for exploring the environment or providing rapid response to directional cues, but that the lamella is important for productive cell movement.

skTM displaced Arp2/3 and cofilin, normally concentrated in the lamellipodium, and increased F-actin concentration. The displacement of Arp2/3 and cofilin is consistent with the ability of TMs to block the actin branching or severing activities of these proteins in vitro (Bernstein and Bamburg, 1982; Blanchoin et al., 2001; DesMarais et al., 2002), whereas increased F-actin may be due TM's ability to prevent pointed end depolymerization in vitro (Broschat, 1990). The loss of Arp2/3 and cofilin correlated with decreased concentration of free barbed filament ends at the cell edge and the loss of the narrow, rapidly treadmilling actin array. This finding suggests that Arp2/3 and cofilin mediate the lamellipodium kinetic signature. Arp2/3's involvement in this was corroborated by its inhibition with CA. Inhibition of the lamellipodium by both skTM or CA promoted filopodial protrusions, suggesting that filopodia can arise by an Arp2/3-independent pathway, such as filament elongation mediated by Mena/VASP (Lebrand et al., 2004).

skTM also enhanced myosin II concentration in the lamella and promoted its accumulation at the cell edge where it is normally excluded. The increased myosin concentration correlated with increased F-actin convergence between the lamella and cell body. This suggests that myosin II recruited to F-actin by skTM was active, which is consistent with structural studies in which activated myosin II bound to skTM-saturated F-actin in the absence of troponin (Lehman et al., 1995). skTM also promoted the rapid formation and turnover of substrate adhesions closer to the cell edge. This is likely

Table II. skTM increases protrusion persistence and cell migration rates

	Control cells	skTM cells	CA cells
Protrusion time	28.3 ± 2.9 s $n = 28$ measurements 8 cells	58.7 ± 7.9 s $n = 30$ measurements 10 cells P = 0.0009	28.5 ± 2.6s $n = 68$ measurements 15 cells P = 0.09
Retraction time	49.8 ± 7.4 s $n = 32$ measurements 8 cells	27.6 ± 3.2 s $n = 30$ measurements 10 cells P = 0.002	42.4 ± 4.7s $n = 66$ measurements 15 cells P = 0.2
Protrusion rate	0.69 ± 0.06 mm/min $n = 81$ measurements 8 cells	0.88 ± 0.14 mm/min $n = 36$ measurements 10 cells P = 0.3	0.23 ± 0.2 mm/min $n = 68$ measurements 15 cells P = 0.08
Retraction rate	0.58 ± 0.06 mm/min $n = 64$ measurements 8 cells	0.53 ± 0.07 $n = 26$ measurements 10 cells P = 0.66	0.13 ± 0.01 mm/min $n = 66$ measurements 15 cells P = 0.06
Protrusion initiation frequency	0.85/min	2.4/min	1.0/min
Retraction initiation frequency	2.8/min	0.86/min	1.2/min
Cell migration rate	0.59 ± 0.01 mm/min $n = 73$ cells	1.22 ± 0.02 mm/min $n = 113$ cells P < 0.0001	0.48 ± 0.01 mm/min $n = 9$ cells

Quantification of leading edge dynamics was made from kymographs of phase-contrast image series acquired at 10-s intervals (Fig. 6). Cell migration rates were measured from the position of the nucleus over time in phase-contrast image series acquired at 2-min intervals. Numbers are averages ± SEM.

not a direct effect of skTM on integrin activation but a product of enhanced actomyosin promotion of substrate adhesion turnover (Chrzanowska-Wodnicka and Burridge, 1996; Webb et al., 2004). Paxillin punctae were also along central F-actin bundles in cells containing skTM, suggesting that faster migration of these cells was due to increased engagement of myosin II contractility along F-actin bundles spanning between the lamella and cell body, which were engaged to the substrate at sites along their length, allowing the cell to pull itself forward more efficiently.

How does the leading edge of cells lacking a lamellipodium still move forward? One possibility is that increased contraction in the cell center and rear could squeeze a pliant leading edge forward by hydrostatic pressure, as may occur in leukocyte or amoeboid movement (Hartwig et al., 1983; Fukui, 1993). However, this possibility disagrees with our microrheo-

logical demonstration of increased stiffness in the lamella and our EM analysis showing increased density and bundling of filaments in the lamella of cells containing skTM. Leading edge protrusion in cells containing skTM still requires actin polymerization from barbed ends because protrusion was blocked by cytochalasin D (Fig. 4 G). Thus, there must be either an alternative Arp2/3- and ADF/cofilin-independent mechanism for barbed-end production, sufficient preexisting barbed ends that are protected from capping, or enough residual Arp2/3 and ADF/cofilin activity to allow adequate actin polymerization for leading edge protrusion. This could be mediated by a "leaky cap" such as formin or Mena/Vasp protected filaments (Bear et al., 2002; Zigmond, 2004). Filament elongation likely occurs from stiff skTM-coated (Kojima et al., 1994) and myosin II–cross-linked lamella F-actin, whose rigidity would allow monomer addition at the leading edge to overcome membrane
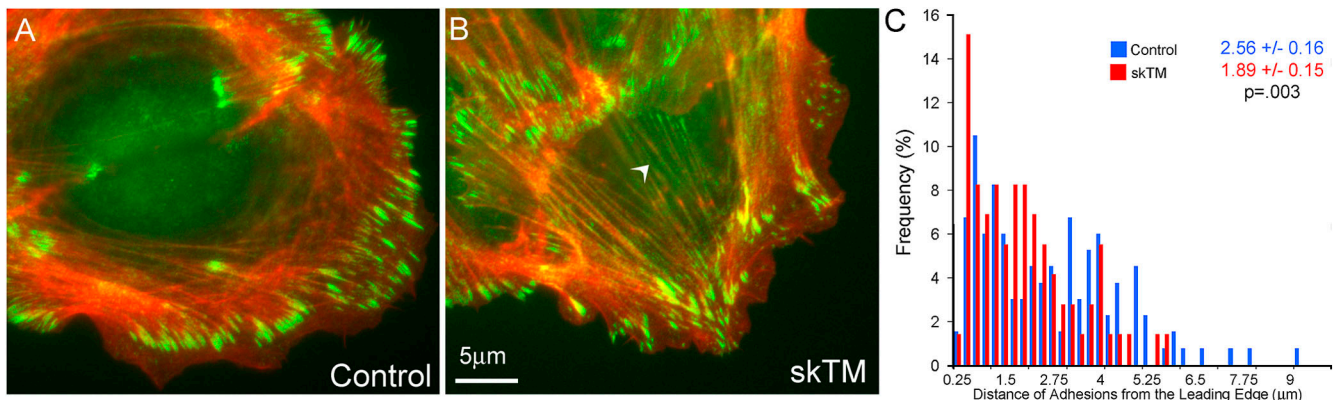

Figure 7. **Substrate adhesions form closer to the leading edge in cells containing skTM.** F-actin staining (fluorescent phalloidin, red) and paxillin immunolocalization (green) in control (A) and skTM-injected (B) cells. Arrowhead in B shows paxillin punctae along central F-actin bundles that are not present in F-actin in A. (C) Frequency histogram of the distance of the distal-most border of paxillin foci from the leading edge in control and skTM-injected cells ($n = 8$ cells, 10–15 measurements per cell per treatment). Numbers in the top right of graph are the mean distance (± SEM) of the adhesion sites from the cell edge.

Figure 8. **skTM enhances the stiffness of the lamella.** Phase-contrast micrographs of a control cell (A) and an skTM-injected cell (B) overlaid marks corresponding to the positions of fluorescent microspheres that were injected into the cell. Particle loci are color coded according to the local value of the cytoplasmic elasticity from red (softest) to blue (stiffest). (C) Relative elasticity of the cell body (CB) and lamella (LM) of control and TM-injected cells calculated at a sampling frequency of 1 Hz. Graph shows mean elasticity ($\pm$ SEM); differences in elasticity are significant (P < 0.05).
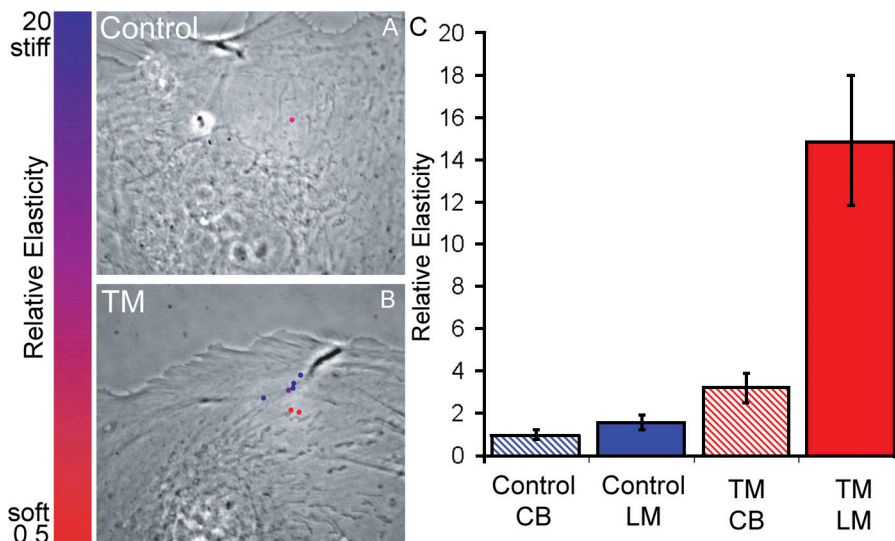
tension as is thought to occur in the dendritic meshwork assembly model (Mullins et al., 1998; Mogilner and Oster, 2003). Indeed, studies of *Listeria monocytogenes* and bead motility in vitro have shown that a dendritic meshwork is not necessary for polymerization-based propulsion if the F-actin is cross-linked by proteins such as fascin or α-actinin (Brieher et al., 2004) or polymerization is mediated by mdia (Romero et al., 2004).

Long TMs organize and maintain contraction

Inhibition of endogenous long TM function by TM311 antibody injection changed the contractile and protrusive behavior of the cell in ways that contrasted the effects induced by excess skTM. Long TM inhibition reduced F-actin convergence and induced misdirected protrusions with low directional persistence. In contrast, skTM-containing cells showed enhanced F-actin convergence and protrusion persistence. Thus, endogenous long TMs are likely critical to

organizing actomyosin and promoting contraction in central cell regions, which in turn restricts lamellipodium formation to a specific persistent site at the cell edge. Previous studies suggest different isoforms of TMs segregate spatially, which may lead to spatial and functional specialization of subsets of the F-actin cytoskeleton, as occurs in cell migration (Temm-Grove et al., 1998; Bryce et al., 2003). Thus, we suggest TM is important for regionally defining the molecular, kinetic, and kinematic properties of the actin cytoskeleton, which can mediate changes in cell morphology and migration.

Materials and methods

Cell culture and microinjection
PtK$_1$ cells were cultured as described previously (Wittmann et al., 2003). X-rhodamine–conjugated actin was prepared as described previously (Waterman-Storer, 2002) and microinjected into cells at 1 mg/ml. Rabbit skeletal muscle TM (predominately αTM) was purified from psoas muscle as de-
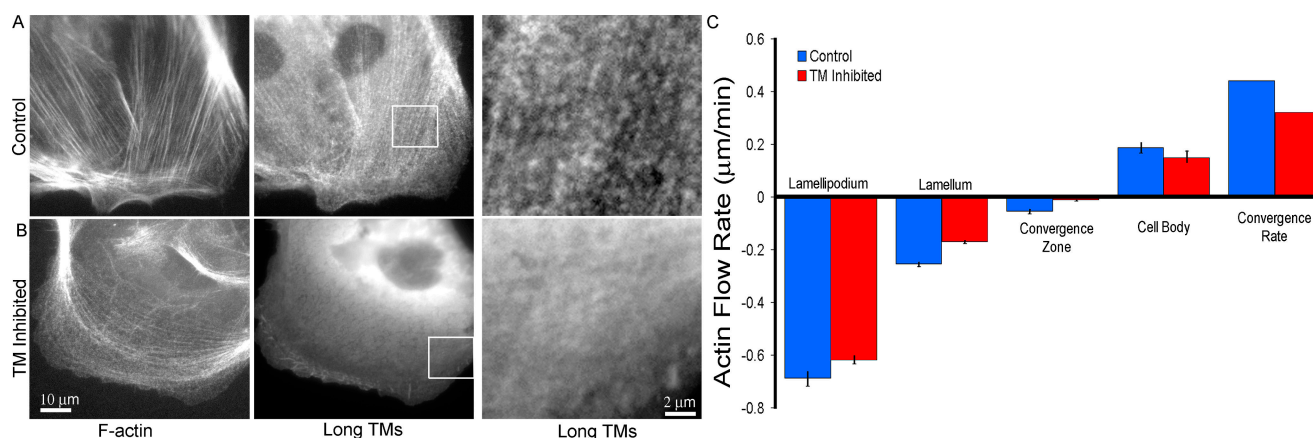

Figure 9. **Antibody inhibition of long TM isoforms displaces TM from F-actin and decreases myosin II–dependent F-actin convergence.** (A and B) F-actin (fluorescent phalloidin) and long isoforms of TM (TM 311 antibody) in control (A) and cells injected with TM311 antibody (B). In control cells, long TM localizes along F-actin bundles, but is displaced from F-actin bundles in TM311 antibody–injected cells. Right column shows a magnified view of TM in the boxed regions. (C) Average F-actin flow rates $\pm$ SEM in control and TM311-injected cells with negative and positive rates indicating retrograde and anterograde flow, respectively.

scribed previously (Bailey, 1948) and microinjected at 140 μM. TM311 antibody (Sigma-Aldrich) was microinjected at 1 mg/ml. For experiments requiring expression of GFP-labeled proteins, fluorescent actin, skTM, and the DNA plasmid at 1 mg/ml were comicroinjected into the nucleus.

Live cell and immunofluorescence microscopy
Cells were maintained on the microscope stage at 37°C with an air stream incubator (Nevtek) in aluminum chambers (Wittmann et al., 2003) in culture medium containing 30 μl oxyrase per milliliter of media (Oxyrase, Inc.) to inhibit photobleaching.

F-actin FSM, GFP fluorescence, and phase-contrast time-lapse image series were acquired at 5- to 10-s intervals using a 100 × 1.4 NA Plan Apo phase-contrast objective lens (Nikon) on a spinning disk confocal scanner (Yokogawa) described in Adams et al. (2003). For drug treatments, cells were imaged in a stainless steel perfusion chamber (Gupton and Waterman-Storer, 2005) and treated with either 100 μM blebbistatin or 200 nM cytochalasin D.

Leading edge activity and cell migration rates were determined from phase-contrast time series acquired on an inverted microscope (model TE300; Nikon) equipped with electronically controlled shutters and a robotic stage with linear position feedback encoders on the x, y, and z axes (model MS-2000; Applied Scientific Instruments). Images were acquired on a 12-bit cooled CCD camera (model Orca 285; Hamamatsu) controlled by MetaMorph software (Universal Imaging Corp.) using a 20 × 0.5 NA Plan Apo phase-contrast objective lens (Nikon). For cell velocity measurements, images were captured every 2 min for 5 h, whereas for leading edge characterization images were taken every 10 s for 10 min.

Epifluorescence images of fixed cells were acquired on an inverted microscope (model TE300 Quantum; Nikon) equipped with a triple band pass dichroic mirror and a 14-bit cooled CCD camera (model Orca II; Hamamatsu) controlled by MetaMorph software using a 60×/1.4 NA Plan Apo DIC objective lens (Nikon).

Immunofluorescence and quantification of polymerization-competent free barbed ends
Control and skTM-injected cells were fixed in cytoskeletal buffer (10 mM MES, 3mM MgCl$_2$, 138 mM KCl, and 2 mM EGTA, pH 6.9) containing 4% PFA, permeabilized in cytoskeletal buffer containing 0.5% Triton X-100, and immunolabeled for the following: long isoforms of TM (TM311; Sigma-Aldrich); all TM isoforms (polyclonal RB14; Ursitti and Fowler, 1994); injected rabbit skeletal muscle TM (CH1; Sigma-Aldrich), paxillin (Signal Transduction Laboratories), mDia2 (a gift from A. Alberts, Van Andel Research Institute, Grand Rapids, MI), Mena and VASP (a gift from F. Gertler, Massachusetts Institute of Technology, Cambridge, MA), ADF/cofilin (Cytoskeleton), or Arp3 (a gift from M. Welch, University of California, Berkeley, Berkeley, CA) using the appropriate fluorescently labeled secondary antibodies (Jackson ImmunoResearch Laboratories). For myosin IIA heavy chain immunofluorescence (Biomedical Technologies, Inc.), cells were processed as previously described (Cramer and Mitchison, 1995). F-actin was labeled with fluorescent phalloidin. To localize and quantify the relative number of actin filament free barbed ends, live cells were permeabilized with 0.25 mg/ml saponin in the presence of 0.5 μM X-rhodamine actin and fixed as previously described (Symons and Mitchison, 1991).

Image analysis and quantification
F-actin flow rates in each cellular region were measured by kymograph analysis as previously described (Salmon et al., 2002). F-actin polymerization and depolymerization maps were calculated using qFSM software (Ponti et al., 2003; Vallotton et al., 2003). In brief, this software identifies F-actin speckles as diffraction-limited intensity peaks that are significantly different from image noise. Speckle appearance, intensity fluctuations, and time of disappearance are then determined to allow calculation of maps of the relative rates of actin filament depolymerization and polymerization. The output of this algorithm represents polymerization in a red scale and depolymerization in a green scale, with bright red and bright green depicting fast polymerization and fast depolymerization, respectively.

To analyze immunofluorescence data, fluorescence intensity was measured along multiple 50-pixel-wide regions (three to four per cell spaced at even intervals along leading edge) normal to the leading edge from the cell edge into the cell center. The averages from multiple regions in multiple cells were calculated and plotted against distance from the leading edge. The distance between the distal border of substrate adhesions and cell edge was measured from paxillin immunofluorescence images. All measurements were made from controls and skTM-injected cells plated on the same coverslip.

For kymograph analysis of leading edge behavior, four to eight ran-

domly placed lines normal to the free cell edge were used. Leading edge protrusion and retraction rates, frequencies of switching between phases, and time of protrusion or retraction persistence were calculated from these kymographs. Velocities of cells in small islands (3–6 cells/island) comprised exclusively of either controls, skTM-injected cells, or CA-expressing cells were measured using the track objects function in MetaMorph.

Intracellular cytomechanics using particle tracking microrheology
The intracellular elasticity was measured using the method of particle tracking microrheology introduced by Tseng et al. (2002). 100-nm-diam carboxylated fluorescent polystyrene nanospheres (Molecular Probes) were microinjected into cells with or without skTM (Kole et al., 2004). Movies of the thermally excited Brownian displacements of the beads were recorded by time-lapse microscopy using a CCD camera (model Orca II; Hamamatsu) on an epifluorescence microscope (model TE300; Nikon). The coordinates of the particles' centroids were monitored with a spatial resolution of ∼10 nm and a temporal resolution of 0.1 s and transformed into mean square displacements using a subroutine incorporated into MetaMorph. Mean square displacements were mathematically transformed into a local cytoplasmic elasticity (Mason et al., 1997), which describes the propensity of the local network in the vicinity of the probe nanospheres to resist the random mechanical stresses generated by the Brownian motion.

Immunoblot analysis
PtK1 cells were lysed in sample buffer and subjected to SDS-PAGE followed by immunoblotting. The CG3 mAb reacts with the exon 1b–encoded NH$_2$ terminus products of the TM5 gene in short nonmuscle TMs (a gift from J. Lin, University of Iowa, Iowa City, IA; Lin et al., 1985), the CH1 monoclonal reacts with striated muscle TM (Lin et al., 1985), the RB14 polyclonal recognizes all TM isoforms, and the TM311 monoclonal (Sigma-Aldrich) recognizes an epitope within residues 14–32 in all long TM isoforms but doesn't cross-react with short TMs (Nicholson-Flynn et al., 1996).

Electron microscopy
PtK$_1$ cells were grown for 5 d on carbon-coated formvar 100 mesh finder grids (EMS). Control cells and skTM-injected cells were fixed in 100 mM Pipes, pH 6.9, 1 mM MgSO$_4$, 1 mM EGTA buffer containing 2% PFA, and 0.05% glutaraldehyde, washed, and stained with aqueous 2% OsO$_4$ and 2% uranyl acetate. Dehydration in increasing concentrations of reagent grade ethanol (15, 20, 50, 70, 95, and 100%; 3 min per change) was followed by critical-point drying according to Anderson (1951) and Buckley and Porter (1975). Images were obtained under low-dose conditions using a microscope (model Tecnai 12; FEI electron optics) equipped with a Lab$_6$ filament (Denka) at 120 kV. Tilt angles from ±15 to ±20° were used for the stereo-pair images. Kodak SO-163 plates were developed for 13 min in (1:1) D19 developer (Eastman Kodak Co.).

Online supplemental material
Fig. S1 depicts stereo pairs showing a portion of the leading edge of control and skTM-injected cells from the same cell cluster. Fig. S2 shows that Mena, VASP, and mDia2 localization are similar in control and skTM-injected cells. Fig. S3 shows that high levels of skTM do not alter filamin and cortactin distribution. Video 1 shows that cells containing skTM exhibit only one region of F-actin kinematic behavior at their leading edges. Video 2 shows that high levels of skTM inhibit the kinetic signature of the lamellipodium. Video 3 shows that high levels of skTM induce multiple filopodial protrusions from the cell edge. Video 4 shows that high levels of skTM induce changes in distribution and dynamics of paxillin containing substrate adhesions. Video 5 shows that cells with inhibited TM exhibit decreased lamellipodial protrusion persistence. The online supplemental material is available at http://www.jcb.org/cgi/content/full/jcb. 200406063/DC1.

References

Adams, M.C., W.C. Salmon, S.L. Gupton, C.S. Cohan, T. Wittmann, N. Prigozhina, and C.M. Waterman-Storer. 2003. A high-speed multispectral spinning-disk confocal microscope system for fluorescent speckle microscopy of living cells. *Methods.* 29:29–41.

Anderson, T.F. 1951. Techniques for the preservation of three-dimensional structure in preparing specimens. *EM. Trans. NY Acad. Sci.* 13:130–134.

Apgar, J., Y. Tseng, E. Federov, M.B. Herwig, S.C. Almo, and D. Wirtz. 2000. Multiple-particle tracking measurements of heterogeneities in solutions of actin filaments and actin bundles. *Biophys. J.* 79:1095–1106.

Bailey, K. 1948. Tropomyosin—a new asymmetric protein component of the muscle fibril. *Biochem. J.* 43:271–287.

Bailly, M., F. Macaluso, M. Cammer, A. Chan, J.E. Segall, and J.S. Condeelis. 1999. Relationship between Arp2/3 complex and the barbed ends of actin filaments at the leading edge of carcinoma cells after epidermal growth factor stimulation. *J. Cell Biol.* 145:331–345.

Bear, J.E., T.M. Svitkina, M. Krause, D.A. Schafer, J.J. Loureiro, G.A. Strasser, I.V. Maly, O.Y. Chaga, J.A. Cooper, G.G. Borisy, and F.B. Gertler. 2002. Antagonism between Ena/VASP proteins and actin filament capping regulates fibroblast motility. *Cell.* 109:509–521.

Bernstein, B.W., and J.R. Bamburg. 1982. Tropomyosin binding to F-actin protects the F-actin from disassembly by brain actin-depolymerizing factor (ADF). *Cell Motil.* 2:1–8.

Blanchoin, L., T.D. Pollard, and S.E. Hitchcock-DeGregori. 2001. Inhibition of the Arp2/3 complex-nucleated actin polymerization and branch formation by tropomyosin. *Curr. Biol.* 11:1300–1304.

Brieher, W.M., M. Coughlin, and T.J. Mitchison. 2004. Fascin-mediated propulsion of *Listeria monocytogenes* independent of frequent nucleation by the Arp2/3 complex. *J. Cell Biol.* 165:233–242.

Broschat, K.O. 1990. Tropomyosin prevents depolymerization of actin filaments from the pointed end. *J. Biol. Chem.* 265:21323–21329.

Bryce, N.S., G. Schevzov, V. Ferguson, J.M. Percival, J.J. Lin, F. Matsumura, J.R. Bamburg, P.L. Jeffrey, E.C. Hardeman, P. Gunning, and R.P. Weinberger. 2003. Specification of actin filament function and molecular composition by tropomyosin isoforms. *Mol. Biol. Cell.* 14:1002–1016.

Buckley, I.K., and K.R. Porter. 1975. Electron microscopy of critical point dried whole cultured cells. *J. Microsc.* 104:107–120.

Carlier, M.F., V. Laurent, J. Santolini, R. Melki, D. Didry, G.X. Xia, Y. Hong, N.H. Chua, and D. Pantaloni. 1997. Actin depolymerizing factor (ADF/cofilin) enhances the rate of filament turnover: implication in actin-based motility. *J. Cell Biol.* 136:1307–1322.

Chrzanowska-Wodnicka, M., and K. Burridge. 1996. Rho-stimulated contractility drives the formation of stress fibers and focal adhesions. *J. Cell Biol.* 133:1403–1415.

Cramer, L.P., and T.J. Mitchison. 1995. Myosin is involved in postmitotic cell spreading. *J. Cell Biol.* 131:179–189.

Danuser, G., and C.M. Waterman-Storer. 2003. Quantitative fluorescent speckle microscopy: where it came from and where it is going. *J. Microsc.* 211: 191–207.

Dasgupta, B.R., S.Y. Tee, J.C. Crocker, B.J. Frisken, and D.A. Weitz. 2002. Microrheology of polyethylene oxide using diffusing wave spectroscopy and single scattering. *Phys. Rev. E Stat. Nonlin. Soft Matter Phys.* 65:051505.

DesMarais, V., I. Ichetovkin, J. Condeelis, and S.E. Hitchcock-DeGregori. 2002. Spatial regulation of actin dynamics: a tropomyosin-free, actin-rich compartment at the leading edge. *J. Cell Sci.* 115:4649–4660.

Fukui, Y. 1993. Toward a new concept of cell motility: cytoskeletal dynamics in amoeboid movement and cell division. *Int. Rev. Cytol.* 144:85–127.

Gupton, S.L., and C.M. Waterman-Storer. 2005. Live-cell fluorescent speckle microscopy of actin cytoskeletal dynamics and their perturbation by drug perfusion. *In* Cell Biology: A Laboratory Handbook. Vol. 3. J.E. Celis, editor. Academic Press Inc., Orlando, FL. In press.

Gupton, S.L., W.C. Salmon, and C.M. Waterman-Storer. 2002. Converging populations of f-actin promote breakage of associated microtubules to spatially regulate microtubule turnover in migrating cells. *Curr. Biol.* 12:1891–1899.

Hartwig, J.H., H.L. Yin, and T.P. Stossel. 1983. How phagocytic leukocytes move. *J. Clin. Chem. Clin. Biochem.* 21:535–544.

Ichetovkin, I., W. Grant, and J. Condeelis. 2002. Cofilin produces newly polymerized actin filaments that are preferred for dendritic nucleation by the Arp2/3 complex. *Curr. Biol.* 12:79–84.

Izzard, C.S., and L.R. Lochner. 1980. Formation of cell-to-substrate contacts during fibroblast motility: an interference-reflexion study. *J. Cell Sci.* 42:81–116.

Kojima, H., A. Ishijima, and T. Yanagida. 1994. Direct measurement of stiffness of single actin filaments with and without tropomyosin by in vitro nanomanipulation. *Proc. Natl. Acad. Sci. USA.* 91:12962–12966.

Kole, T.P., Y. Tseng, L. Huang, J.L. Katz, and D. Wirtz. 2004. Rho kinase regulates the intracellular micromechanical response of adherent cells to Rho activation. *Mol. Biol. Cell.* 15:3475–3484.

Lazarides, E. 1976. Two general classes of cytoplasmic actin filaments in tissue culture cells: the role of tropomyosin. *J. Supramol. Struct.* 5:531–563.

Lebrand, C., E.W. Dent, G.A. Strasser, L.M. Lanier, M. Krause, T.M. Svitkina, G.G. Borisy, and F.B. Gertler. 2004. Critical role of Ena/VASP proteins for filopodia formation in neurons and in function downstream of netrin-1. *Neuron.* 42:37–49.

Lehman, W., P. Vibert, P. Uman, and R. Craig. 1995. Steric-blocking by tropomyosin visualized in relaxed vertebrate muscle thin filaments. *J. Mol. Biol.* 251:191–196.

Lin, C.H., E.M. Espreafico, M.S. Mooseker, and P. Forscher. 1996. Myosin drives retrograde F-actin flow in neuronal growth cones. *Neuron.* 16:769–782.

Lin, J.J., C.S. Chou, and J.L. Lin. 1985. Monoclonal antibodies against chicken tropomyosin isoforms: production, characterization, and application. *Hybridoma.* 4:223–242.

Lin, J.J., K.S. Warren, D.D. Wamboldt, T. Wang, and J.L. Lin. 1997. Tropomyosin isoforms in nonmuscle cells. *Int. Rev. Cytol.* 170:1–38.

Mason, T.G., K. Ganesan, J.H. van Zanten, D. Wirtz, and S.C. Kuo. 1997. Particle tracking microrheology of complex fluids. *Phys. Rev. Lett.* 79:3282–3285.

Mogilner, A., and G. Oster. 2003. Force generation by actin polymerization II: the elastic ratchet and tethered filaments. *Biophys. J.* 84:1591–1605.

Mullins, R.D., J.A. Heuser, and T.D. Pollard. 1998. The interaction of Arp2/3 complex with actin: nucleation, high affinity pointed end capping, and formation of branching networks of filaments. *Proc. Natl. Acad. Sci. USA.* 95:6181–6186.

Nicholson-Flynn, K., S.E. Hitchcock-DeGregori, and P. Levitt. 1996. Restricted expression of the actin-regulatory protein, tropomyosin, defines distinct boundaries, evaginating neuroepithelium, and choroid plexus forerunners during early CNS development. *J. Neurosci.* 16:6853–6863.

Pollard, T.D., L. Blanchoin, and R.D. Mullins. 2000. Molecular mechanisms controlling actin filament dynamics in nonmuscle cells. *Annu. Rev. Biophys. Biomol. Struct.* 29:545–576.

Ponti, A., P. Vallotton, W.C. Salmon, C.M. Waterman-Storer, and G. Danuser. 2003. Computational analysis of F-actin turnover in cortical actin meshworks using fluorescent speckle microscopy. *Biophys. J.* 84:3336–3352.

Ponti, A., M. Machacek, S.L. Gupton, C.M. Waterman-Storer, and G. Danuser. 2004. Two distinct actin networks drive the protrusion of migrating cells. *Science.* 305:1782–1786.

Romero, S., C. Le Clainche, D. Didry, C. Egile, D. Pantaloni, and M.F. Carlier. 2004. Formin is a processive motor that requires profilin to accelerate actin assembly and associated ATP hydrolysis. *Cell.* 119:419–429.

Salmon, W.C., M.C. Adams, and C.M. Waterman-Storer. 2002. Dual-wavelength fluorescent speckle microscopy reveals coupling of microtubule and actin movements in migrating cells. *J. Cell Biol.* 158:31–37.

Strasser, G.A., N.A. Rahim, K.E. VanderWaal, F.B. Gertler, and L.M. Lanier. 2004. Arp2/3 is a negative regulator of growth cone translocation. *Neuron.* 43:81–94.

Svitkina, T.M., and G.G. Borisy. 1999. Arp2/3 complex and actin depolymerizing factor/cofilin in dendritic organization and treadmilling of actin filament array in lamellipodia. *J. Cell Biol.* 145:1009–1026.

Symons, M.H., and T.J. Mitchison. 1991. Control of actin polymerization in live and permeabilized fibroblasts. *J. Cell Biol.* 114:503–513.

Temm-Grove, C.J., B.M. Jockusch, R.P. Weinberger, G. Schevzov, and D.M. Helfman. 1998. Distinct localizations of tropomyosin isoforms in LLC-PK1 epithelial cells suggests specialized function at cell-cell adhesions. *Cell Motil. Cytoskeleton.* 40:393–407.

Tilney, L.G., E.M. Bonder, and D.J. DeRosier. 1981. Actin filaments elongate from their membrane-associated ends. *J. Cell Biol.* 90:485–494.

Tseng, Y., T.P. Kole, and D. Wirtz. 2002. Micromechanical mapping of live cells by multiple-particle-tracking microrheology. *Biophys. J.* 83:3162–3176.

Ursitti, J.A., and V.M. Fowler. 1994. Immunolocalization of tropomodulin, tropomyosin and actin in spread human erythrocyte skeletons. *J. Cell Sci.* 107:1633–1639.

Vallotton, P., A. Ponti, C.M. Waterman-Storer, E.D. Salmon, and G. Danuser. 2003. Recovery, visualization, and analysis of actin and tubulin polymer flow in live cells: a fluorescent speckle microscopy study. *Biophys. J.* 85:1289–1306.

Verkhovsky, A.B., T.M. Svitkina, and G.G. Borisy. 1995. Myosin II filament assemblies in the active lamella of fibroblasts: their morphogenesis and role in the formation of actin filament bundles. *J. Cell Biol.* 131:989–1002.

Watanabe, N., and T.J. Mitchison. 2002. Single-molecule speckle analysis of actin filament turnover in lamellipodia. *Science.* 295:1083–1086.

Waterman-Storer, C. 2002. Fluorescent speckle microscopy (FSM) of microtubules and actin in living cells. *In* Current Protocols in Cell Biology. John Wiley & Sons, Inc., Hoboken, NJ. 4.10.1–4.10.26.

Waterman-Storer, C.M., A. Desai, J.C. Bulinski, and E.D. Salmon. 1998. Fluorescent speckle microscopy, a method to visualize the dynamics of protein assemblies in living cells. *Curr. Biol.* 8:1227–1230.

Webb, D.J., K. Donais, L.A. Whitmore, S.M. Thomas, C.E. Turner, J.T. Parsons, and A.F. Horwitz. 2004. FAK-Src signalling through paxillin, ERK and MLCK regulates adhesion disassembly. *Nat. Cell Biol.* 6:154–161.

Welch, M.D., A.H. DePace, S. Verma, A. Iwamatsu, and T.J. Mitchison. 1997. The human Arp2/3 complex is composed of evolutionarily conserved subunits and is localized to cellular regions of dynamic actin filament assembly. *J. Cell Biol.* 138:375–384.

Wittmann, T., G.M. Bokoch, and C.M. Waterman-Storer. 2003. Regulation of leading edge microtubule and actin dynamics downstream of Rac1. *J. Cell Biol.* 161:845–851.

Zigmond, S.H. 2004. Formin-induced nucleation of actin filaments. *Curr. Opin. Cell Biol.* 16:99–105.